Exposure to ambient black carbon derived from a unique inventory and high-resolution model

Rong Wang[a,b], Shu Tao[a,b,1], Yves Balkanski[c], Philippe Ciais[b,c], Olivier Boucher[d], Junfeng Liu[a], Shilong Piao[a,b], Huizhong Shen[a], Maria Raffaella Vuolo[c], Myrto Valari[e], Han Chen[a], Yuanchen Chen[a], Anne Cozic[c], Ye Huang[a], Bengang Li[a], Wei Li[a], Guofeng Shen[a], Bin Wang[a], and Yanyan Zhang[a]

[a]Laboratory for Earth Surface Processes, College of Urban and Environmental Sciences, and [b]Sino-French Institute for Earth System Science, Peking University, Beijing 100871, China; [c]Laboratoire des Sciences du Climat et de l'Environnement, Commissariat à l'Energie Atomique-Centre National de la Recherche Scientifique-Université de Versailles Saint-Quentin-en-Yvelines, Centre d'Etudes Orme des Merisiers, 91191 Gif sur Yvette, France; [d]Laboratoire de Météorologie Dynamique, Institut Pierre Simon Laplace-Centre National de la Recherche Scientifique, Université Pierre et Marie Curie, 75252 Paris Cedex 05, France; and [e]Laboratoire de Météorologie Dynamique, Institut Pierre Simon Laplace-Centre National de la Recherche Scientifique, Ecole Polytechnique, 91128 Palaiseau Cedex, France

Edited by A. R. Ravishankara, Chemical Sciences Division, National Oceanic and Atmospheric Administration Earth System Research Laboratory, Boulder, CO, and approved December 12, 2013 (received for review October 4, 2013)

Black carbon (BC) is increasingly recognized as a significant air pollutant with harmful effects on human health, either in its own right or as a carrier of other chemicals. The adverse impact is of particular concern in those developing regions with high emissions and a growing population density. The results of recent studies indicate that BC emissions could be underestimated by a factor of 2–3 and this is particularly true for the hot-spot Asian region. Here we present a unique inventory at 10-km resolution based on a recently published global fuel consumption data product and updated emission factor measurements. The unique inventory is coupled to an Asia-nested (~50 km) atmospheric model and used to calculate the global population exposure to BC with fully quantified uncertainty. Evaluating the modeled surface BC concentrations against observations reveals great improvement. The bias is reduced from −88% to −35% in Asia when the unique inventory and higher-resolution model replace a previous inventory combined with a coarse-resolution model. The bias can be further reduced to −12% by downscaling to 10 km using emission as a proxy. Our estimated global population-weighted BC exposure concentration constrained by observations is 2.14 μg·m^{-3}; 130% higher than that obtained using less detailed inventories and low-resolution models.

air pollution | climate change | model resolution | emission inventory

Black carbon (BC), or soot, emitted from incomplete combustion of carbonaceous fuels is an air pollutant which also plays an important role in climate change (1). BC is an indicator of air particulate pollution and BC in ambient air has an impact on human health (2). In a recent study in China, it was found that the effects of BC on morbidity appear to be more robust than the effects of fine particles in general (3, 4).

However, global atmospheric aerosol models often underestimate the concentration of BC at the surface, particularly over Asia, by a factor that typically ranges from 2 to 10 (5–7). In one study, the observed BC surface concentration for China could only be reproduced by doubling the emissions prescribed to a transport model (8). It is often argued that the underestimation is due to a low bias in BC emission inventories, suggesting a need to revisit these previous inventories (9).

In a bottom-up approach, BC emission is estimated based on the amount of fuel consumed and an emission factor (EF_{BC}, defined as the amount of BC emitted per unit mass of fuel consumed) for each of various combustion sources. For previous inventories, the lack of EF_{BC} measurements in developing countries led to high uncertainty in estimating the total emissions (10). In addition, the use of fuel data at the national level is likely to distort the geographical distribution of emissions within large countries such as China and India (11). Recently, a 0.1° × 0.1° fuel database with 64 types of combustion has been developed based on local or national fuel consumption statistics. This database improves the resolution of the spatial distribution of emissions for large countries (12). To fill the data gap in developing countries, a set of EF_{BC} values has been compiled for various residential solid fuel combustion devices and vehicles (13–20). In addition to the problems with the emission inventories, the coarse resolution of existing global aerosol models also hinders our ability to capture detailed spatial variation, leading to poor agreement between model prediction and observations (7).

In this study we develop and evaluate a unique global BC emission inventory using a zoomed aerosol model, and estimate the global population's exposure to BC with a focus on Asia. The influence of model resolution and the use of an updated emission inventory on the calculated BC concentration are evaluated against field observations.

Updated BC Emission Inventory

Based on an updated EF_{BC} dataset (21, 22) and a recently published 0.1° × 0.1° fuel consumption data product (12), we have drawn up a global 0.1° × 0.1° BC inventory for 2007 [Peking University BC Inventory for 2007 (PKU-BC-2007)] (*Methods*). According to PKU-BC-2007, the global total and anthropogenic-only BC emission in 2007 was 8.9 and 6.3 Tg, respectively. Asia contributed 4.1 Tg of the total and 3.8 Tg of the anthropogenic BC. A Monte Carlo simulation, varying the parameters of PKU-BC-2007, yields an interquartile range (IQR) of 5.4–14.8 Tg for global annual BC emission. The IQR would be 5.6–14.4 Tg if

Significance

In this study, we have developed a unique global black carbon (BC) emission inventory using a 10-km grid based on the latest source and emission factor information. The inventory is used to model BC concentrations using a global atmospheric aerosol climate model, with a high-resolution grid for Asia, to better resolve the exposure of populations to elevated BC concentration. The model with even higher resolution (10 km) is used for the North China Plain. Finally, the population exposure concentrations are evaluated.

Author contributions: S.T. designed research; R.W., H.S., M.V., H.C., Y.C., Y.H., W.L., G.S., B.W., and Y.Z. performed research; M.R.V., M.V., and A.C. contributed new reagents/analytic tools; R.W., S.T., Y.B., P.C., O.B., J.L., S.P., H.C., and B.L. analyzed data; and R.W. and S.T. wrote the paper.

The authors declare no conflict of interest.

This article is a PNAS Direct Submission.

[1]To whom correspondence should be addressed. E-mail: taos@pku.edu.cn.

This article contains supporting information online at www.pnas.org/lookup/suppl/doi:10.1073/pnas.1318763111/-/DCSupplemental.

only variation in EF_{BC} had been considered, indicating that the overall uncertainty is dominated by errors in EF_{BC}. A similar result has been found previously by Lu et al. (23). The probability distributions of BC emissions for major sources are shown in Fig. S1.

The global total emission and emissions from China and India derived here are compared with those previously reported in Table S1. The update of EF_{BC} and the use of local fuel data result in global emission from energy-related sources in PKU-BC-2007 (6.3 Tg) being ~30% higher than in previous inventories (average of 4.9 ± 0.4 Tg) (7, 11, 24–27). In addition to the differences in total emission, the spatial patterns of emission also differ markedly between them. Fig. 1 shows the global distribution of BC emissions in PKU-BC-2007 and its comparison with MACCity (MACC/CityZEN EU projects), an inventory created for the Atmospheric Chemistry and Climate Model Intercomparison Project in support of the Fifth Assessment Report of the Intergovernmental Panel on Climate Change (11, 24). The largest underestimation by MACCity is found in the north and southwest of China, as well as in the northeast of India, where carbon-based fuels are used intensively in the residential sector in rural areas. The main reason for such differences comes from the fact that the unique inventory takes into account subnational fuel consumption data (12), whereas MACCity is based on national fuel data, and thus implicitly assumes per capita fuel consumption is uniformly spread over each country. The subnational fuel consumption data indicate that the hypothesis that per capita fuel consumptions are equal over each country is far from true.

BC Concentrations in Surface Air

The performance of the new inventory in combination with high-resolution modeling is evaluated by comparing PKU-BC-2007 with MACCity, and two versions of LMDZORINCA (LMDZ for Laboratoire de Météorologie Dynamique, OR for Organizing Carbon and Hydrology in Dynamic Ecosystems, and INCA for Interactions between Aerosols and Chemistry) (28), an Asia-zoomed model (INCA-zA, 0.51° × 0.66° over Asia and 4.62° × 4.64° for other regions) and a regular-grid model of coarser resolution (INCA, 1.27° × 2.5° globally). The four inventory/model combinations compared are thus PKU-BC-2007/INCA-zA (E_{PKU}/M_{INz}), MACCity/INCA-zA (E_{MAC}/M_{INz}), PKU-BC-2007/INCA (E_{PKU}/M_{IN}), and MACCity/INCA (E_{MAC}/M_{IN}), where E indicates the emission inventory and M indicates the model version. The model meteorological fields are obtained by nudging the winds from the meteorological reanalysis data produced by the European Centre for Medium-Range Weather Forecasts (29). This technique allows for simulated meteorological fields closely related to observed ones. The three quartiles of the emissions in PKU-BC-2007 are prescribed in the model. BC concentrations are calculated based on the medians (the second quartiles), whereas the uncertainties in the estimates are quantified by a range of BC concentrations calculated based on the first and the third quartiles. Fig. 2 shows the comparison of calculated surface BC concentration (annual mean for 2007) against in situ measurements made at 229 stations (all of them measured during 2003–2010 with five exceptions measured during 1999–2002 in Asia). Observations from different years are used to ensure a more extensive validation, assuming that year-to-year BC variations at one site are smaller than the spatial gradients between sites used for validation. The spatial distribution of observation sites is shown in Fig. S2 and detailed information is provided in Table S2. Generally, use of the new inventory gives a better agreement with observations. The normalized mean bias (NMB) is calculated for each of the four combinations. The lowest NMB is achieved by E_{PKU}/M_{INz} for Asia, and E_{PKU}/M_{IN} for the rest of the world. For Asian sites, the NMB is reduced from −88% for E_{MAC}/M_{IN} down to −35% for E_{PKU}/M_{INz}, whereas the percentage of sites with deviations of the modeled concentrations from the observations less than a factor of 2 increases from 24% to 73%. When the first and third quartiles of PKU-BC-2007 are prescribed, the NMBs become −59% and −7%, respectively. It is worth noting that a significant reduction in the bias between modeled and measured BC concentrations is achieved at severely polluted stations. As an example, the average BC concentration measured over the North China Plain (NCP) (13 sites) is 7.33 $\mu g \cdot m^{-3}$, far closer to the 5.31 $\mu g \cdot m^{-3}$ estimated by E_{PKU}/M_{INz} than to the 2.14 $\mu g \cdot m^{-3}$ by E_{MAC}/M_{IN}. However, in regions other than Asia, the improvement is not so significant, with NMB only reduced from 50% (E_{MAC}/M_{IN}) to 48% (E_{PKU}/M_{IN}), likely due to the coarser model resolution. Finally, the all-site NMB can be reduced to −45% if E_{PKU}/M_{INz} is used for Asia and E_{PKU}/M_{IN} is used for other regions, in comparison with −58% if only using E_{MAC}/M_{IN}.

In addition, using PKU-BC-2007 gives modeled vertical profiles of BC mass mixing ratios (Fig. S3) and seasonality of surface BC concentrations (Fig. S4) which compared satisfactorily to observations. Even though E_{PKU}/M_{INz} provides the best results out of the four combinations tested over Asia, this combination still underestimates BC. One likely reason is that emissions and BC concentrations are heterogeneous even across densely populated grid cells of 50 km, the best resolution of E_{PKU}/M_{INz}. To test this hypothesis, surface BC concentrations in the NCP region (marked in Fig. 1*A*) are explicitly modeled with a state-of-the-art model, CHIMERE (30), at the original resolution of the PKU-BC-2007 inventory, i.e., 0.1° × 0.1°. The results of this most realistic simulation are compared with those from INCA and INCA-zA against 13 observations available in Fig. S5. For these sites, the NMBs are reduced from −71% (E_{PKU}/M_{IN}) to −29% (E_{PKU}/M_{INz}) and −8% (E_{PKU}/CHIMERE), indicating a strong influence of model resolution. Note that the greatest improvements occur in heavily polluted areas, suggesting that the high-resolution model can better catch the detailed spatial variation compared with the coarse-resolution model.

Unfortunately 0.1° × 0.1° resolution modeling of atmospheric BC concentration, as has been done here with CHIMERE in the NCP region, can hardly be applied globally; the computational load would be too great. Instead, an emission density-based nonlinear downscaling method is developed by assuming that the subgrid spatial distribution of surface BC concentrations is related to that of the underlying BC emissions. Thus, BC concentrations

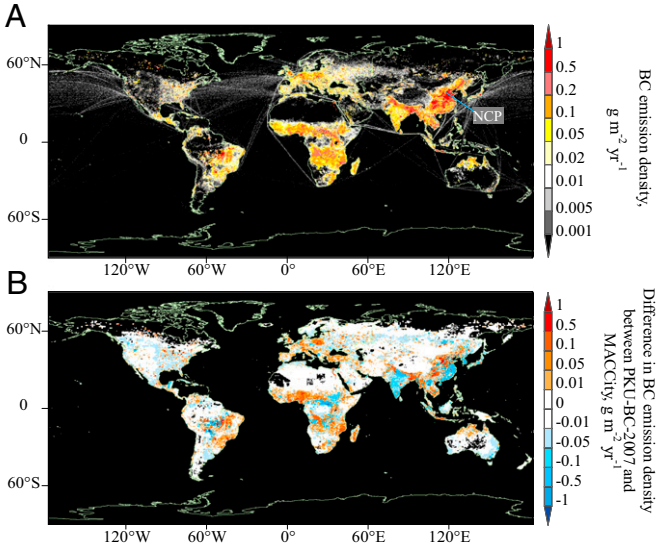

Fig. 1. Global distribution of BC emissions in 2007. (*A*) The 0.1° × 0.1° distribution of BC emissions by PKU-BC-2007. (*B*) Difference between the PKU-BC-2007 (downscaled to 0.5° × 0.5°) and MACCity (2007, 0.5° × 0.5°) inventories.

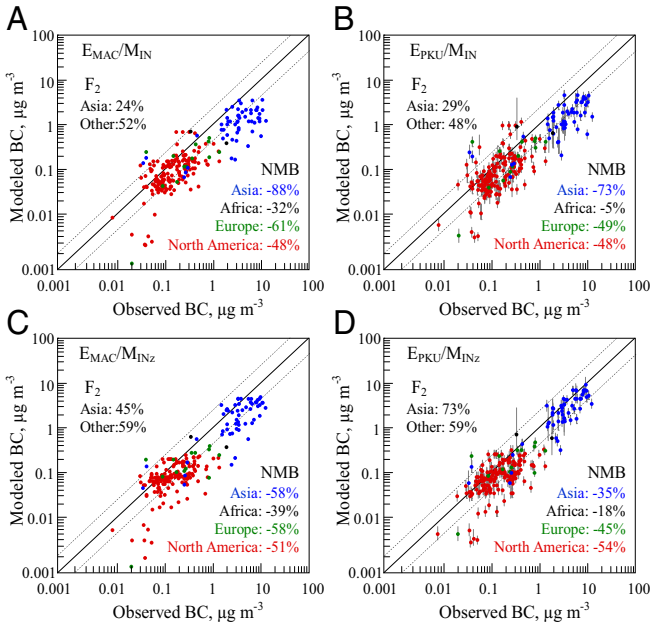

Fig. 2. Comparison between the modeled and observed surface BC concentrations for the four inventory/model combinations. (*A*) E_{MAC}/M_{IN}. (*B*) E_{PKU}/M_{IN}. (*C*) E_{MAC}/M_{INz}. (*D*) E_{PKU}/M_{INz}. The sites in Asia (blue), Africa (black), Europe (green), and North America (red) are marked with different colors. Error bars (vertical lines) are derived by using the first and the third quartiles of PKU-BC-2007 as inputs. NMB is given for each region. The dashed lines show the range of a factor of two deviation of the modeled concentration from the observation and percentages of sites with deviations less than a factor of 2 (F_2) are listed.

modeled by E_{PKU}/M_{INz} and E_{PKU}/M_{IN} are downscaled to 0.1° × 0.1° using emission density as a proxy (*Methods*), and then compared with that explicitly modeled by E_{PKU}/CHIMERE. An exponent (α) is introduced to address the influence of the dispersion of subgrid scale emissions (*Methods*). The optimal value of α (0.30) is derived by a trial-and-error method to achieve the lowest mean deviation between calculated and observed BC concentrations at 55 sites in Asia and 174 sites in the rest of the world (Fig. S6). Using this downscaling method, the residual low bias of the model is substantially reduced for both Asia and other regions. Although the exponent can implicitly account for dispersion in a simplified way, the influence of transport within each model grid cell could not be fully resolved by the downscaling method.

Population Inhalation Exposure to Ambient BC

These results suggest that realistic BC concentrations downscaled to 10 km can be better modeled by using the combination of the E_{PKU}/M_{INz} in Asia and E_{PKU}/M_{IN} elsewhere, together with the emission-based nonlinear downscaling. The resulting surface ambient BC concentrations are converted into population-weighted exposure concentrations. Fig. 3 shows the spatial distribution of these exposure concentrations at 0.1° × 0.1° in 2007. The geographical distribution of the exposure concentrations is similar to that of the emission, due to the short atmospheric lifetime of BC. Because emission sources and population covary spatially, the global average population exposure concentration (2.14 μg·m^{-3}) is significantly higher than the global average surface concentration in ambient air (0.28 μg·m^{-3}). The high-exposure areas are located in the densely populated areas of East Asia and South Asia (Fig. 3 *B* and *C*). The annual mean BC exposure concentrations in the NCP (China), Sichuan Basin (China), and Indo-Gangetic Plain (India) are as high as 6.68, 5.49, and 4.31 μg·m^{-3}, respectively. In these regions, a total of 1.02 Tg BC were emitted in 2007, primarily from the domestic burning of biomass fuel (44%) and coal (20%) and from coke production (19%), motor vehicles (9%), and brick kilns (6%). Extremely high BC exposure (>6 μg·m^{-3}) can be found in metropolitan areas with a population density over 1,000 per km^2 (Fig. 3 *B* and *C*).

Fig. 4 shows the global and regional cumulative frequency distributions of ambient BC exposure concentration. People in East Asia are exposed to a much higher BC concentration than those in other regions. According to Geng et al. (3), in Shanghai, China, for an IQR increase of ambient BC concentration from 2.2 to 4.9 μg·m^{-3}, the cardiovascular, respiratory, and total mortality of the population increase by 3.2%, 0.6%, and 2.3%, and emergency-room and outpatient visits increase 1.33% and 3.35%, respectively. It appears that the percentages of people exposed to an annual mean BC concentration above 4.9 μg·m^{-3} in East Asia and South Asia are as high as 18% and 11%, respectively, suggesting a relatively high health risk which cannot yet be quantified.

As with the modeled concentrations at measurement sites, the calculated exposure concentrations are influenced significantly by inventory and model resolution. Fig. 5 compares the average BC concentrations modeled at monitoring sites and the regional average exposure concentrations derived by the four inventory/model combinations without downscaling and by the two combinations with downscaling [$(E_{PKU}/M_{INz})_d$ and $(E_{PKU}/M_{IN})_d$, where $_d$ indicates the downscaling method) in East Asia, South Asia, Europe, and North America. When the estimate resolution is increased from ~200 km (E_{PKU}/M_{IN}) or ~50 km (E_{PKU}/M_{INz}) to ~10 km, the model-calculated BC concentrations at the monitoring sites approach the observations. With downscaling, the calculated results agree well with the observations (100–104%), except in Europe (61%) where the low bias is due to the relatively coarse model resolution of INCA. Simultaneously, the

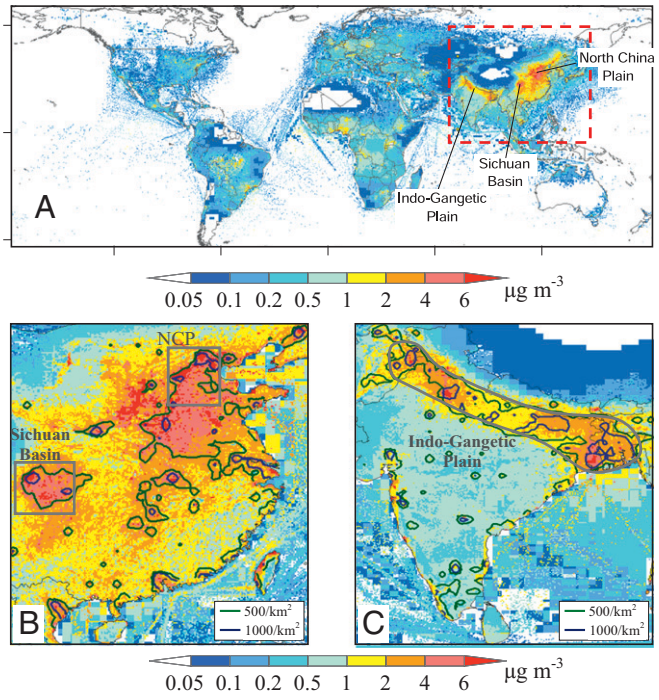

Fig. 3. Spatial distribution of population exposure to BC concentrations for the (*A*) world, (*B*) East Asia, and (*C*) South Asia. The concentrations are derived by downscaling the results from E_{PKU}/M_{INz} in Asia and from E_{PKU}/M_{IN} in the other regions to 0.1° × 0.1° grids using emission as a proxy. Contours in *B* and *C* denote population density.

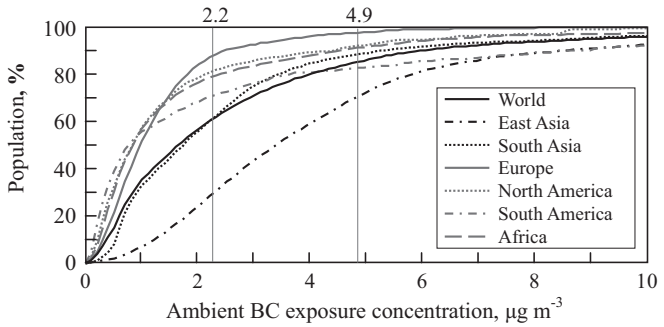

Fig. 4. Cumulative frequency distributions of BC exposure in different regions. The BC concentrations are derived by downscaling the results given by E_{PKU}/M_{INz} in Asia and by E_{PKU}/M_{IN} in the other regions to 0.1° × 0.1° grids using emission as a proxy.

exposure concentrations increase dramatically. The four model/inventory combinations without downscaling would underestimate the exposure risk by 30–67% for these regions. If the combination of E_{MAC}/M_{IN} were used, the calculated average exposure concentration in Asia would be as low as 1.52 μg·m^{-3}, compared with 2.12 and 3.39 μg·m^{-3} by E_{PKU}/M_{INz} without and with downscaling. In Europe and North America, the exposure concentrations would increase by 80% and 110%, respectively, after downscaling (from ∼200 to ∼10 km). In addition, for the 5% of the most vulnerable population, the exposure concentrations are equal to or higher than 6.72 μg·m^{-3} in India and 10.4 μg·m^{-3} in China, which would be underestimated as 2.21 and 4.33 μg·m^{-3} if the combination of E_{MAC}/M_{IN} were to be used.

Conclusion

The levels of population exposure to ambient air BC estimated in this study are higher than those previously documented for several reasons: (*i*) the unique BC emission inventory derived from the recently published fuel consumption data product and updated EF_{BC} database, (*ii*) modeling with higher resolution in Asia, and (*iii*) downscaling to rectify the bias caused by the covariance of emission and population at resolution higher than the model resolution. It is demonstrated that the exposure of populations living in hot spots is diluted and the population-weighted concentration is reduced when a coarse model resolution is applied and the population exposure could be underestimated by an insufficiently fine-resolution model. Although it is demonstrated in this study that downscaling can help reduce the bias, direct calculation using a finer-resolution model (10 km or higher) would be preferred for drawing up future assessments of the exposure and risk of BC, as well as other short-lived air pollutants.

The need for high-resolution inventories and atmospheric models illustrated by this study will become even more critical for health impact studies when accelerated urbanization in developing countries causes populations to become more unevenly distributed in the future. It is predicted that the urban population of China and India will respectively increase from 42% and 29% of the population in 2007 up to 62% and 40% in 2030 (31). If BC concentrations were stable, urbanization alone would cause population exposure to increase by 15% and 14% in China and India, respectively, due to factors of 2.1 and 3.0 differences in the exposure concentrations between urban and rural populations.

Methods

Development of the BC Emission Inventory. The global 0.1° × 0.1° BC emission inventory PKU-BC-2007 is based on a global fuel combustion database (PKU-FUEL-2007) (12) and an updated EF_{BC} database (*SI Methods*). A total of 706 EF_{BC} data measured in 13 countries from 1985 to 2011 were included (Table S3), including up-to-date measurements, particularly for developing countries. The technical-split method is applied for 16 combustion processes including coal combustion in power plants and industrial boilers, brick kilns, coke production, motor vehicles, residential firewood, residential coal, and agricultural waste combustion (Tables S4 and S5). A 1,000-point Monte Carlo approach is applied to characterize the uncertainty. Detailed information for developing the inventory is provided in *SI Methods*.

Atmospheric Models of BC. The global aerosol model LMDZORINCA and the regional off-line chemistry-transport model CHIMERE are used to calculate the 4D distributions of BC concentrations. These models are briefly introduced here and more details are presented in the literature (28, 30, 32). LMDZORINCA is a global aerosol model that couples a general circulation model (Laboratoire de Météorologie Dynamique) to an aerosol module (Interactions between Aerosols and Chemistry) (28, 32). A zoomed version is run at a resolution of 0.51° in latitude and 0.66° in longitude for a region of 50–130°E, 0–55°N centered over China and India, whereas a regular version is run at a fixed resolution of 1.27° × 2.50°. The same vertical coordinates are used in the two versions with 19 vertical layers from 3.88 to 1,013 hPa. For CHIMERE, the latest version (30) is run at a horizontal resolution of 0.1° × 0.1° with 8 vertical layers in hybrid sigma-pressure coordinates for a domain over the NCP (113°S:120°E, 36°N:42°N), driven by 0.1° × 0.1° meteorological data from Weather Research and Forecasting Model (30). In CHIMERE, BC is divided into nine size bins, and major aerosol dynamics, dry deposition, and wet scavenging are considered for BC (30).

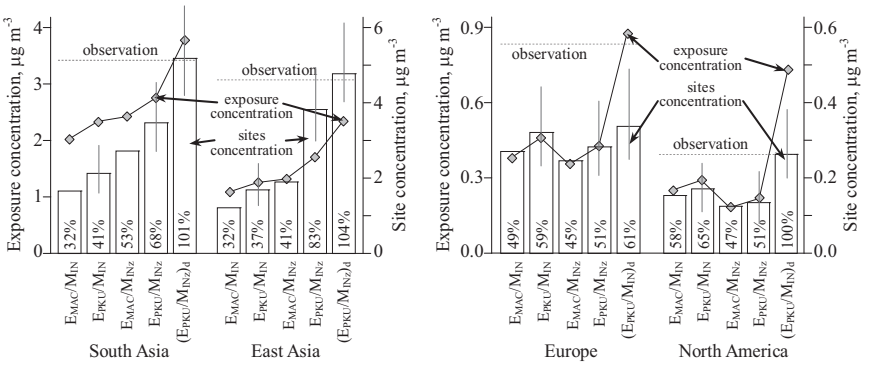

Fig. 5. Comparison of the calculated surface-air BC concentrations at observation sites and population exposure concentrations in four regions of South Asia, East Asia, Europe, and North America among different methods. The methods compared are four inventory/model combinations (E_{MAC}/M_{IN}, E_{PKU}/M_{IN}, E_{MAC}/M_{INz}, and E_{PKU}/M_{INz}) and the two with downscaling [$(E_{PKU}/M_{INz})_d$ for E_{PKU}/M_{INz} and $(E_{PKU}/M_{IN})_d$ for E_{PKU}/M_{IN}]. The model-calculated average surface-air concentrations at all observation sites are shown as bars, which are compared with the observed mean concentrations (dashed lines) by the marked percentages (modeled concentrations divided by observed ones). Error bars for individual bars are derived by using the first and the third quartiles of PKU-BC-2007 as inputs, which represent the uncertainty range of modeled surface BC concentrations resulting from the uncertainty in emissions. The population-weighted BC exposure concentrations at these sites are shown as diamonds.

Downscaling of BC Concentrations to 0.1° × 0.1°. Surface BC concentrations calculated by INCA-zA in Asia and by INCA for the rest of the world are downscaled from the model grid (*x, y*) (0.51° × 0.66° grid in INCA-zA or 1.27° × 2.5° grid in INCA) to a 0.1° × 0.1° subgrid (*i, j*) as

$$C^{*}_{i,j} = C_{x,y}\frac{E^{\alpha}_{i,j}}{\sum_{i,j}\left(F_{i,j}E^{\alpha}_{i,j}\right)},$$

where $C^{*}_{i,j}$ is the downscaled concentration of the subgrid (*i, j*); $C_{x,y}$ is the model-calculated concentration of grid cell (*x, y*); $E_{i,j}$ is the emission density in the subgrid (*i, j*); the exponent α is a seasonal-constant coefficient describing the nonlinear relationship between $C_{x,y}$ and $E_{i,j}$, and is derived from a trial-and-error method to minimize the mean deviation between calculated and observed BC concentrations at 55 sites in Asia and 174 sites in the rest of the world (Fig. S6); $F_{i,j}$ is the fraction of area of each subgrid (*i, j*) in the model grid (*x, y*), and the product of $F_{i,j}$; and $E_{i,j}{}^{\alpha}$ is the area-weighted emission density in the subgrid (*i, j*).

ACKNOWLEDGMENTS. We thank R. Coveney for reviewing the manuscript; J. Gash for proofreading; K. Smith, D. Hauglustaine, and H. D. Han for discussions on exposure estimates; and W. M. Hao for valuable suggestions in writing the manuscript. This work is funded by the National Science Foundation of China (Grant 41390243 and 41130754), the 111 project (B14001), and the Beijing Municipal Government (YB20101000101).

1. Shindell D, et al. (2012) Simultaneously mitigating near-term climate change and improving human health and food security. *Science* 335(6065):183–189.
2. Janssen NAH, et al. (2012) *Health Effects of Black Carbon* (World Health Organization, Copenhagen).
3. Geng F, et al. (2013) Differentiating the associations of black carbon and fine particle with daily mortality in a Chinese city. *Environ Res* 120:27–32.
4. Wang X, et al. (2013) Associations between fine particle, coarse particle, black carbon and hospital visits in a Chinese city. *Sci Total Environ* 458–460:1–6.
5. Koch D, et al. (2009) Evaluation of black carbon estimations in global aerosol models. *Atmos Chem Phys* 9(22):9001–9026.
6. Menon S, et al. (2010) Black carbon aerosols and the third polar ice cap. *Atmos Chem Phys* 10(10):4559–4571.
7. Bond TC, et al. (2013) Bounding the role of black carbon in the climate system: A scientific assessment. *J Geophys Res* 118:5380–5552.
8. Wang Q, et al. (2011) Sources of carbonaceous aerosols and deposited black carbon in the Arctic in winter-spring: Implications for radiative forcing. *Atmos Chem Phys* 11: 12453–12473.
9. Lucas L (2013) New agreement casts spotlight on efforts to inventory black carbon. *ScienceInsider*. Available at http://lucaslaursen.com/clips/sootsurvey.pdf. Accessed January 4, 2014.
10. Bond TC, et al. (2004) A technology-based global inventory of black and organic carbon emissions from combustion. *J Geophys Res* 109:D14203.
11. Lamarque JF, et al. (2010) Historical (1850-2000) gridded anthropogenic and biomass burning emissions of reactive gases and aerosols: Methodology and application. *Atmos Chem Phys* 10(15):7017–7039.
12. Wang R, et al. (2013) High resolution mapping of combustion processes and implications for CO_2 emissions. *Atmos Chem Phys* 13(10):5189–5203.
13. Zhi GR, et al. (2008) Emission characteristics of carbonaceous particles from various residential coal-stoves in China. *Environ Sci Technol* 42(9):3310–3315.
14. Zhang YX, et al. (2008) Characteristics of particulate carbon emissions from real-world Chinese coal combustion. *Environ Sci Technol* 42(14):5068–5073.
15. Bi XH, Simoneit BRT, Sheng GY, Fu JM (2008) Characterization of molecular markers in smoke from residential coal combustion in China. *Fuel* 87:112–119.
16. Li XH, Wang SX, Duan L, Hao JM, Nie YF (2009) Carbonaceous aerosol emissions from household biofuel combustion in China. *Environ Sci Technol* 43(15):6076–6081.
17. Shen GF, et al. (2010) Emission factors of particulate matter and elemental carbon for crop residues and coals burned in typical household stoves in China. *Environ Sci Technol* 44(18):7157–7162.
18. Chen YJ, et al. (2009) Measurements of black and organic carbon emission factors for household coal combustion in China: Implication for emission reduction. *Environ Sci Technol* 43(24):9495–9500.
19. Shen GF, et al. (2012) Emission factors, size distributions, and emission inventories of carbonaceous particulate matter from residential wood combustion in rural China. *Environ Sci Technol* 46(7):4207–4214.
20. Subramanian R, et al. (2009) Climate-relevant properties of diesel particulate emissions: Results from a piggyback study in Bangkok, Thailand. *Environ Sci Technol* 43(11):4213–4218.
21. Wang R, et al. (2012) Black carbon emissions in China from 1949 to 2050. *Environ Sci Technol* 46(14):7595–7603.
22. Wang R, et al. (2012) Global emission of black carbon from motor vehicles from 1960 to 2006. *Environ Sci Technol* 46(2):1278–1284.
23. Lu Z, Zhang Q, Streets DG (2011) Sulfur dioxide and primary carbonaceous aerosol emissions in China and India, 1996-2010. *Atmos Chem Phys* 11:9839–9864.
24. Granier C, et al. (2011) Evolution of anthropogenic and biomass burning emissions of air pollutants at global and regional scales during the 1980-2010 period. *Clim Change* 109:163–190.
25. Dentener F, et al. (2006) Emissions of primary aerosol and precursor gases in the years 2000 and 1750 prescribed data-sets for AEROCOM. *Atmos Chem Phys* 6(12):4321–4344.
26. Junker C, Liousse C (2008) A global emission inventory of carbonaceous aerosol from historic records of fossil fuel and biofuel consumption for the period 1860-1997. *Atmos Chem Phys* 8(5):1195–1207.
27. Bond TC, et al. (2007) Historical emissions of black and organic carbon aerosol from energy-related combustion, 1850-2000. *Global Biogeochem Cycles* 21:GB2018.
28. Szopa S, et al. (2012) Aerosol and ozone changes as forcing for climate evolution between 1850 and 2100. *Clim Dyn* 40:2223–2250.
29. European Centre for Medium-Range Weather Forecasts (2003) Forty-year European reanalysis of the global atmosphere. Available at www.ecmwf.int/products/. Accessed November 6, 2013.
30. Menut L, et al. (2013) CHIMERE 2013: A model for regional atmospheric composition modelling. *Geosci Model Dev* 6:981–1028.
31. United Nations Department of Economic and Social Affairs (2011) World population prospects: The 2010 revision. Available at http://esa.un.org/wpp/Documentation/pdf/WPP2010_Volume-I_Comprehensive-Tables.pdf. Accessed January 4, 2014.
32. Hourdin F, et al. (2006) The LMDZ4 general circulation model: climate performance and sensitivity to parametrized physics with emphasis on tropical convection. *Clim Dyn* 27(7-8):787–813.